Research Article | Vol. 11, No. 12 / 1 December 2020 / Biomedical Optics Express 7286
Biomedical Optics EXPRESS

Laser-induced optical breakdown effects of micro-lens arrays and diffractive optical elements on *ex vivo* porcine skin after 1064 nm picosecond laser irradiation

Hyeonsoo Kim,[1] Jewan Kaiser Hwang,[2] Minjung Jung,[3] Jongman Choi,[1,4] and Hyun Wook Kang[1,5,*]

[1]*Industry 4.0 Convergence Bionics Engineering, Pukyong National University, Busan, Republic of Korea*
[2]*Mymirae Research Institute for Dermatologic Science, Seoul, Republic of Korea*
[3]*Department of Pathology, Kosin University Hospital, Busan, Republic of Korea*
[4]*Research and Development, Bluecore Company, Busan, Republic of Korea*
[5]*Department of Biomedical Engineering, Pukyong National University, Busan, Republic of Korea*
[*]*wkang@pukyong.ac.kr*

Abstract: The current study aims to investigate the effects of micro-lens arrays (MLA) and diffractive optical elements (DOE) on skin tissue via intra-dermal laser-induced optical breakdown (LIOB) after irradiation of 1064-nm picosecond laser light at high energy settings. Irradiation with MLA and DOE was tested on dimming paper, tissue-mimicking phantom, and dark pigmented porcine skin to quantitatively compare distributions of micro-beams, micro-bubbles, and laser-induced vacuoles in the skin. DOE yielded more uniform distributions of the micro-beams on the paper and laser-induced micro-bubbles in the phantom, compared to MLA. The *ex vivo* skin test confirmed that the DOE-assisted irradiation accompanied more homogeneous generation of the micro-beams on the tissue surface (deviation of ≤ 3%) and a high density of small laser-induced vacuoles (~78 μm) in the dermis than the MLA-assisted irradiation (deviation of ~26% and ~163 μm). The DOE-assisted picosecond laser irradiation may help to achieve deep and uniformly-generated vacuolization under the basal membrane after intra-dermal LIOB for effective fractional skin treatment.

1. Introduction

Melasma is a pigmentary disorder that occurs primarily on the face with brown or gray patches. The pigmented skin disease is generally attributed to various factors including genetic predispositions, pregnancy, hormonal dysfunction, and exposure to ultraviolet (UV) light. However, the pathogenesis of the melasma is not fully understood yet [1–3]. The melasma occurs in all the cultures and human race but happens more frequently with Fitzpatrick skin types IV to VI because the Fitzpatrick skin types contain more pigmented phenotypes than other skin types [2]. Several therapeutic methods have been performed to treat the melasma, including surgical incision, medical drug, radiofrequency, and laser treatment [1]. Among various treatment methods, high power laser application has been adopted as a popular means to treat the melasma by physically fragmenting skin pigments because of non-invasiveness, rapid treatment time, and short wound recovery [4,5]. Thus, a number of Q-switched nanosecond laser systems with various wavelengths (532, 755, and 1064 nm) and pulse durations (10~100 ns) have been developed and clinically examined to maximize the therapeutic outcomes for the melasma treatment [6]. However, the nanosecond pulse durations are often longer than the thermal relaxation times (10~30 ns) of the melasma pigments, leading to the partial thermal decomposition of the pigments and unfavorable thermal injury to the surrounding skin [7].

#410991 https://doi.org/10.1364/BOE.410991
Journal © 2020 Received 24 Sep 2020; revised 10 Nov 2020; accepted 17 Nov 2020; published 23 Nov 2020

Biomedical Optics EXPRESS

Recently, technological advances introduced picosecond laser systems to the field of dermatology to enhance clinical outcomes of pigmented skin treatment [8]. Unlike conventional nanosecond laser systems, the picosecond lasers with shorter pulse durations (hundreds of 10^{-12} s) yield high irradiances and thus induce high temperature (15,000 K) and high pressure (2 GPa) through multiphoton ionization in skin, which is called laser-induced optical breakdown (LIOB) [9]. LIOB is a non-linear absorption process that leads to generation of plasma at the irradiance threshold of 10^2~10^4 GW/cm^2 or higher (i.e., sub-nanosecond regime) in skin [10]. As a result, high temperature and high pressure during LIOB can accompany plasma expansion with audible acoustic signatures and shockwave propagation, leading to vacuolization inside the skin [9]. In turn, the LIOB-associated picosecond laser systems can be more beneficial to achieving fragmentation and complete thermal decomposition of small pigments via collective mechanisms (photomechanical and photothermal), compared to the existing nanosecond laser systems. Therefore, the clinical goal of the pigmented skin treatment with the picosecond lasers is to create vacuoles uniformly in the epidermal and dermal layers via the laser-induced plasma and thus to ablate small target pigments consistently with minimal thermal injury to the adjacent tissue [11].

For fractional skin treatment, a picosecond laser is often used with micro-array lens (MLA) to generate multiple micro-beams and to preserve surrounding skin tissue with minimal thermal injury, compared to a bare beam [12]. However, due to inherent optical features of non-uniform beam distributions, MLA often concentrates the maximum light intensity at the center of a macro-beam with decreasing intensities at both tails [13]. A previous *ex vivo* study demonstrated that the MLA-assisted 1064 nm picosecond laser at low energy settings ($\leq$ 2.1 mJ/micro-beam or radiant exposure = 2.8 J/cm^2) induced non-homogenous vacuoles unevenly dispersed in the epidermis (100~150 μm) through intra-epidermal LIOB, which could hardly treat deeply-located melanin pigments near the basal membrane (300~500 μm) [13,14]. Clinical studies reported a wide range of the laser-induced vacuoles dispersed in human epidermis (50~100 μm) at H_0 = 1.2 J/cm^2 [14,15]. The vacuoles were still shallowly distributed in the epidermis. As a holographic beam splitter, diffractive optical elements (DOE) are also employed to produce multiple micro-beams in various patterns for optical imaging [16]. DOE initially homogenizes the incident laser light and reduces the incident light energy, leading to the uniform distributions of the micro-beams [16]. In spite of the energy loss, the light homogenization can help DOE achieve more constant delivery of the micro-beams to the target in a uniform distribution. The homogeneity of the beam distribution strongly depends on the focal length of DOE and the incident wavelength [17]. However, *ex vivo* studies visualized and reported that the DOE-assisted picosecond laser treatment induced consistently small vacuoles (~50 μm) that were merely confined to the human epidermis [18,19] Thus, the insufficient pulse energy from the picosecond laser often circumvents the application of DOE for the fractional laser skin treatment with intra-dermal LIOB.

The purpose of the current study was to comparatively investigate effects of intra-dermal LIOB with MLA and DOE on *ex vivo* pigmented porcine skin tissue after irradiation of 1064-nm picosecond laser light at high energy settings under various treatment conditions. We hypothesized that DOE with inherent optical patterns could yield more uniform spatial distributions of micro-beams and laser-induced vacuolization in the skin than MLA, given the same conditions. The significance of the current study thus lies in comparative investigation of the optimal conditions for picosecond laser irradiation with MLA and DOE at high energy settings to induce deep and consistent of small vacuoles in skin tissue for effective melasma treatment. *Ex vivo* porcine skin tissue was tested with the picosecond laser with MLA and DOE at high energy settings to explore both distributions and extent of the laser-induced vacuoles in the epidermal and dermal layers. Histological analysis was performed to compare the skin responses of the intra-dermal LIOB between MLA and DOE in a quantitative manner.

Biomedical Optics EXPRESS

2. Materials and methods

2.1. Light source

A 1064 nm picosecond Nd:YAG laser system (pulse duration = 450 ps at FWHM; Picore, Bluecore company, Busan, Republic of Korea) was employed to induce LIOB events in phantoms and *ex vivo* porcine skin tissue. The laser system delivered a pulse energy of up to 1.1 J (at 1 Hz) to evaluate high energy settings for the potential ablation of deep pigments. Micro-lens array (MLA; focal length = 40 mm, 37 micro-beams, diameter = 4 mm, fused silica; Bluecore company, Busan, Republic of Korea) and diffractive optical elements (DOE; focal length = 40 mm, 49 micro-beams, length = 4 mm, fused silica; Bluecore company, Busan, Republic of Korea) were used to generate multiple micro-beams on the target surface for quantitative comparison. Four different pulse energy levels were tested for MLA (0.19, 0.38, 0.57, and 0.76 J) and DOE (0.24, 0.48, 0.72, and 0.96 J) in order to have the identical energy density on the target surface. The corresponding micro-beam energy (= applied pulse energy / number of micro-beams) ranged from 4.9 to 20.5 mJ/micro-beam (i.e., 5.1~20.5 mJ/micro-beam for MLA vs. 4.9~19.6 mJ/micro-beam for DOE). The macro-beam spot size was 4 mm for both MLA (circular shape) and DOE (rectangular shape). To emulate clinical conditions (e.g., applied energy density and skin texture) [20], various treatment conditions were tested: radiant exposure (H_0) and focal depth (FD). Four different H_0 (1.5, 3.0, 4.5, and 6.0 J/cm^2) and three different FDs (0, 5, and 10 mm) were tested to explore the physical roles of the treatment conditions on the spatial distributions of the micro-beams, micro-bubbles, laser-induced vacuoles in the phantom and skin tissue. It should be noted that FD refers to the focal depth in the air as no mismatch boundary condition was considered. Thus, FD = 0 mm means that the incident micro-beams were focused on the target surface whereas FD = 10 mm represents that MLA and DOE approached the surface by 10 mm (i.e., 10 mm closer distance) to focus the incident micro-beams below the target surface. For all the conditions, LIOB was visually confirmed during the laser irradiation. 4×4 cm^2 black dimming paper was initially used to visualize and characterize two-dimensional (2D) spatial distributions of micro-beams from MLA and DOE on the paper surface under various H_0 and FD conditions. A single picosecond pulse was irradiated on the dimming paper to develop LIOB during the irradiation with MLA and DOE. The irradiated paper surface was then photographed by using a digital camera. Both size and distribution of the laser-induced micro-beams on the paper were quantified by using Image J (National Institute of Health, Bethesda, MD).

2.2. Phantom tests

Tissue-mimicking phantom was prepared for comparative tests by using 10% (w/v) gelatin from porcine skin (gel strength 300, type A; Sigma Aldrich, St, Louis, MO, USA) in 70 °C distilled water. Initially, the gelatin powder was poured into the distilled water, and the mixture was stirred for 25 min. Then, 0.03% w/v melanin (synthetic; Sigma Aldrich, St, Louis, MO, USA) was added to the dissolved mixture as a chromophore. When the melanin was melted sufficiently, the mixture was poured into a mold of 5 cm^3 and stored at 4 °C for 12 hr to complete a solidification process. The prepared transparent phantoms were used to characterize 2D spatial distributions of the micro-beams on the surface as well as the axial distributions of the laser-induced micro-bubbles. To evaluate LIOB-induced responses, a single picosecond pulse with MLA and DOE was irradiated on the tissue-mimicking phantoms under various conditions. Both top-surface and cross-section of each treated phantom were photographed to identify spatial distributions of micro-beam spots and to explore axial distributions of laser-induced micro-bubbles in the phantom. Image J was used to measure both size and depth of all the micro-bubbles for quantitative comparison between MLA and DOE. The overall bubble area inside each macro-beam was measured to comparatively examine the dependence of the micro-bubble formation on the applied H_0 and the beam distribution.

Biomedical Optics EXPRESS

2.3. Ex vivo skin tests

For *ex vivo* tests, dark pigmented minipig skin tissue was procured from CRONEX Corp (Seoul, Republic of Korea) as the scattering of the porcine tissue was comparable to that of human skin (1.10 mm^{-1} for porcine dermis vs. 1.34 mm^{-1} for human dermis at 1064 nm [21,22]). 1064 nm picosecond laser light was irradiated with MLA and DOE on the skin tissue at $H_0 = 3.0$ and 6.0 J/cm^2. The tissue was moved laterally by 10 μm after irradiation of every single pulse, and the total treated length was 200 μm (a total of 20 shots was applied). The overlapped irradiation was applied to evidently visualize spatial distributions of laser-induced vacuolization in the skin. Top-view images were captured to measure the spatial distributions of the micro-beams on the skin surface for quantitative comparison between MLA and DOE. After the *ex vivo* experiments, all the treated tissue samples were fixed in 10% neutral buffered formalin (Sigma Aldrich, St, Louis, MO, USA) for two days, sectioned by 5 μm, and stained with hematoxylin and eosin (H&E). Image J was used to characterize both size and distribution of laser-induced vacuolization inside the tissue. All the histology slides were photographed at 100× and 400× by using an optical microscope (Leica DM500, Leica, Wetzlar, Germany). For non-parametric statistical analysis, the Mann-Whitney U test were performed to compare multiple and two groups, respectively, and $p < 0.05$ was considered statistically significant.

3. Results

Figure 1 compares the spatial beam profiles on the black-colored dimming paper between MLA and DOE under various conditions. According to Fig. 1(a), MLA yielded a circular shape of a macro-beam (4 mm in diameter) consisting of 37 micro-beams whereas DOE created a rectangular shape of a macro-beam (4 mm wide) consisting of 49 micro-beams. Regardless of FD, both MLA and DOE showed that the macro-beam spots became more blotted with increasing H_0. As FD increased, MLA experienced no significant change in the overall micro-beams, but noticeable variations in the micro-beam size were observed from the macro-beam profile. On the other hand, DOE presented an increase in the overall micro-beams with increasing FD. However, all the DOE micro-beam sizes were comparable along the lateral macro-beam for all H_0. Figure 1(b) demonstrates the lateral distributions of the micro-beams irradiated with MLA and DOE at 3.0 J/cm^2 (measured from red dashed lines in Fig. 1(a)). MLA was associated with relatively large deviations (17~41%) in the distributions of the micro-beam sizes for all FDs. The average of the micro-beam sizes corresponded to ~214 μm. In contrast, DOE exhibited relatively small deviations (1~9%) in the distributions of the micro-beam sizes for all FDs. The average DOE micro-beam sizes increased from 229 to 1009 μm with increasing FDs, indicating more FD-dependence. Figure 1(c) validated that the overall MLA micro-beam size was relatively invariant for all FDs, but the overall DOE micro-beam size significantly increased with FD ($p < 0.001$ vs. MLA).

Figure 2 displays ablative responses of tissue-mimicking phantom after generation of LIOB with MLA and DOE under various conditions. Similar to Fig. 1(a), Fig. 2(a) confirms that MLA and DOE produced circular and rectangular shapes of a macro-beam on the phantom surface, respectively. Both MLA and DOE revealed vivid formation of laser-induced micro-bubbles on the phantom surface at FD = 0 mm. However, as FD increased, the physical traces of the micro-bubbles on the surface started to disappear, indicating that the location of the micro-bubbles was situated deeper inside the phantom. Regardless of FD, the micro-bubbles created from MLA and DOE accompanied more blotted areas with increasing H_0 as a result of an increase in the individual micro-bubble size. Figure 2(b) compares both size and distribution of the laser-induced micro-bubbles acquired from the middle line (red dashed line) of the treated phantom surface after irradiation with MLA and DOE at 4.5 J/cm^2. MLA yielded the uneven distributions of the micro-bubbles with large deviations of 33~44%. The maximum micro-bubble size occurred at the center of the MLA macro-beams (average micro-bubble size = ~291 μm), and the overall

Biomedical Optics EXPRESS

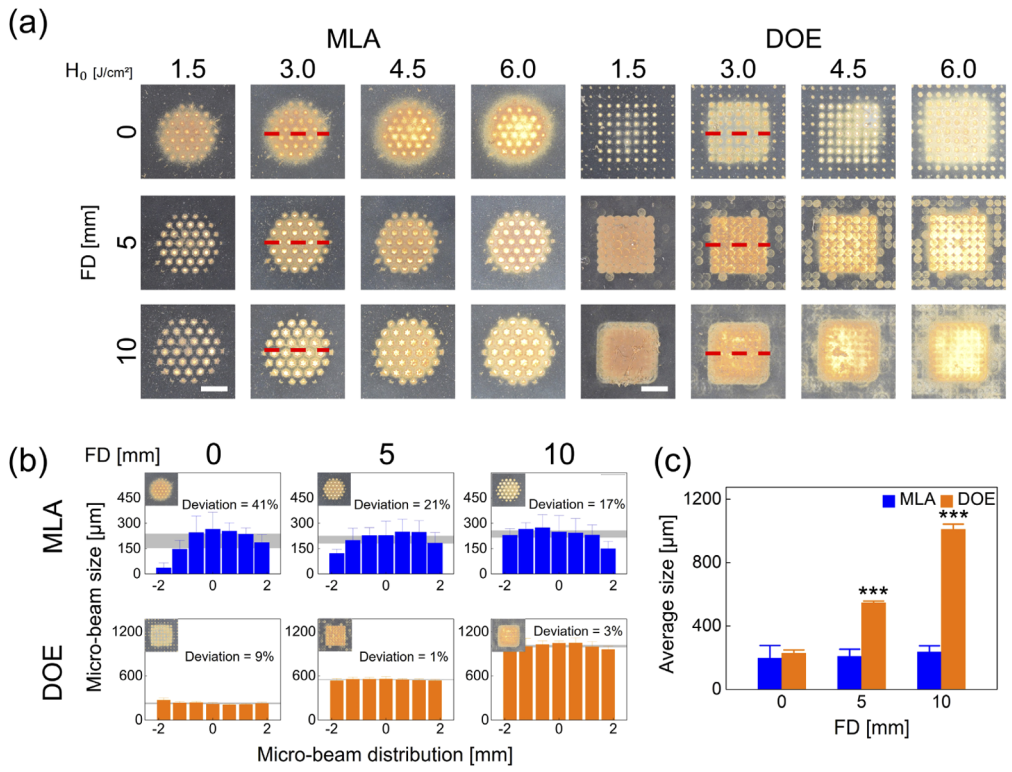

Fig. 1. Comparison of spatial beam profiles between micro-lens arrays (MLA) and diffractive optical elements (DOE) at various radiant exposures (H_0 in J/cm^2) and focal depths (FD in mm): (a) top-view images of macro-beam spots on black-colored dimming paper, (b) spatial distributions of micro-beam sizes acquired from middle line (red dashed line) of macro-beam spots ($H_0 = 3.0$ /cm^2), and (c) overall micro-beam sizes measured from macro-beam spot (bar = 2 mm; ***$p < 0.001$ vs. MLA). Gray areas in (b) represent the deviations for the measured micro-beam sizes.

MLA micro-bubble sizes for all FDs were consistent. On the other hand, DOE generated the uniform distributions of the micro-bubbles with small deviations of 2~5%. The average DOE micro-bubble size increased from 190 to 546 μm with increasing FDs. It is noted that the tendency of the micro-bubbles from MLA and DOE was congruent with that of the micro-beam spots shown in Fig. 1(b). Figure 2(c) exhibits the relative area (coverage in %) of the micro-bubbles generated inside each macro-beam spot at FD = 0 mm (cyan dashed lines in Fig. 2(a)) as a function of H_0 for MLA and DOE. In the case of MLA, the coverage of the micro-bubbles increased slightly with H_0 at FD = 0 mm. In contrast, the DOE-induced micro-bubbles attained a larger coverage of the macro-beam (up to 40%). The bubble coverage from both the groups increased linearly with H_0 at FD = 0 mm ($R^2 = 0.92$).

Figure 3 shows cross-sectional images of laser-treated tissue-mimicking phantoms with MLA and DOE at various conditions. According to Fig. 3(a), the micro-bubble depth increased with H_0 for MLA and DOE. In the case of MLA, the depth also became deeper with increasing FD. The micro-bubble distribution was parabolically fluctuated with the maximum depth occurring at the center of the macro-beam. On the other hand, DOE generated the maximum micro-bubble depth at FD = 5 mm, regardless of H_0. Unlike MLA, the DOE micro-bubble distribution had a flat end-profile for all the conditions. Figure 3(b) compares the axial distributions of the micro-bubbles measured from the cross-sectional images of the laser-treated phantom at various FDs ($H_0 = 4.5$ J/cm^2). Similarly, MLA formed the Gaussian-like distributions (13~74% deviation)

Biomedical Optics EXPRESS

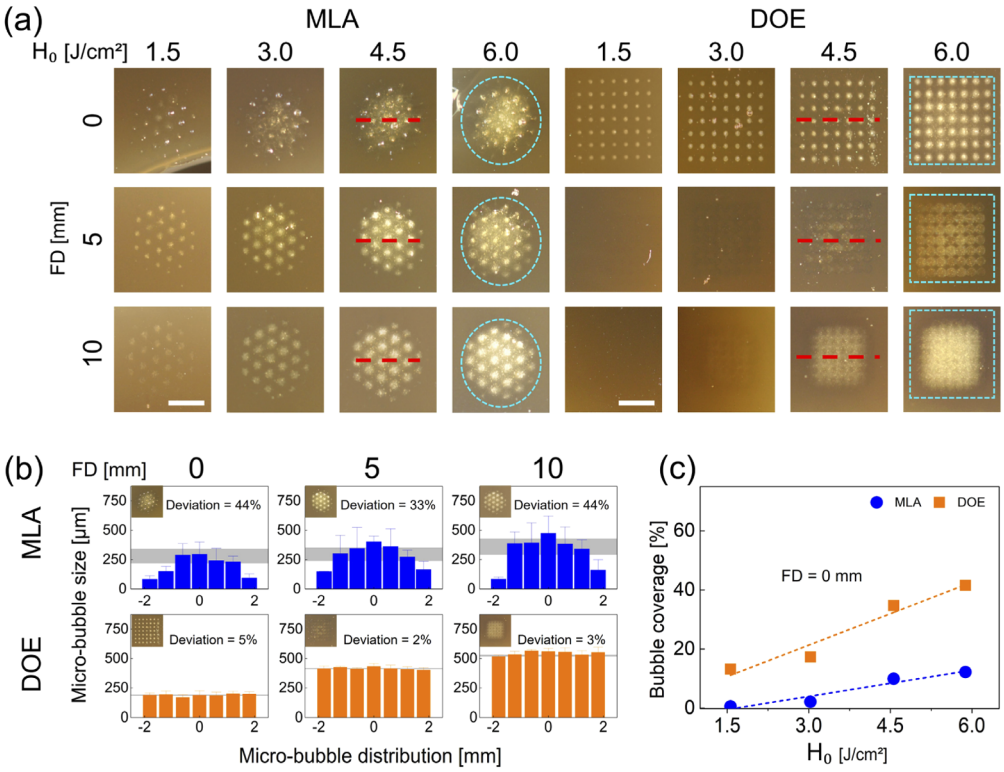

Fig. 2. Evaluations on laser-induced responses of gelatin-based skin mimicking phantom (10% concentration gelatin and 0.03% w/v melanin powder) after irradiation with MLA and DOE at various radiant exposures (H_0 in J/cm^2) and focal depths (FD in mm): (a) top-view images of macro-beam spots (cyan dashed lines) on phantom surface (bar = 2 mm), (b) spatial distributions of micro-bubble sizes acquired from middle line (red dashed line) of macro-beam spots (H_0 = 4.5 /cm^2), and (c) comparison of coverage of micro-bubbles in each macro-beam spot at FD = 0 mm (R^2 = 0.92). Gray areas in (b) represent the deviations for the measured micro-bubble sizes.

of the micro-bubble depths that apparently increased with FD (maximum depth = 7023 μm at FD = 10 mm). However, DOE yielded the flat-top profiles of the micro-bubble depths, and the maximum depth (~5312 μm) occurred at FD = 5 mm with small deviations of 1~5% (vs. 2036 μm at FD = 0 mm and 3142 μm at FD = 10 mm). Figure 3(c) shows the overall micro-bubble depths estimated from MLA and DOE at various conditions. The overall depth from MLA evidently increased with H_0 and FD. Although DOE engendered an increase of the overall micro-bubble depth with H_0, the maximum depth was found consistently at FD = 5 mm. Regardless of H_0 and FD, MLA had large standard deviations in the overall micro-bubble depths because of the non-uniform distribution of the micro-bubbles. In contrast, DOE was still associated with smaller deviations (1~16%) as a result of the axially uniform micro-bubble distributions.

Figure 4 presents *ex vivo* pigmented skin after irradiation with MLA and DOE at various conditions. According to Fig. 4(a), MLA created circular-shaped macro-beam spots on the skin surface while DOE generated rectangular-shaped macro-beam spots, which well corresponded to Figs. 1(a) and 2(a). In the case of MLA, the micro-beam spots became blotted with increasing H_0 and FD. However, DOE showed no significant changes in the micro-beams between 3.0 and 6.0 J/cm^2, but the micro-beam spots increased with FD. Both the groups were associated with superficial thermal lesion (whitish discoloration) on the tissue surface. Figure 4(b) displays

Biomedical Optics EXPRESS

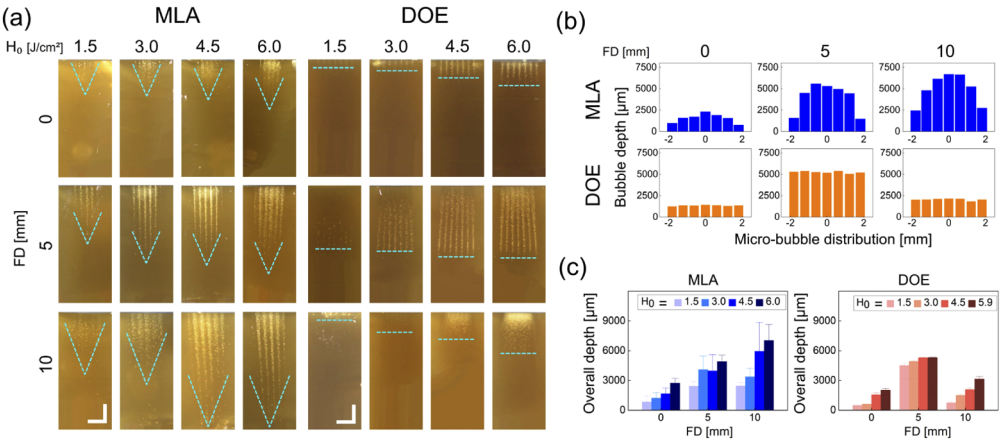

Fig. 3. Evaluations on laser-induced responses of gelatin-based skin mimicking phantom after irradiation with MLA and DOE at various radiant exposures (H_0 in J/cm^2) and focal depths (FD in mm): (a) cross-sectional images of laser-induced micro-bubbles in phantom, (b) axial distributions of micro-bubbles measured at various focal depths (vertical direction; $H_0 = 4.5$ J/cm^2), and (c) quantitative comparison of overall micro-bubble depths between MLA and DOE. Note that cyan dashed lines in (a) indicate the end-profile of the laser-induced micro-bubbles in the phantom (bar = 2 mm)

the lateral distributions of the micro-beams with MLA and DOE irradiated at 3.0 J/cm^2. MLA was associated with relatively large deviations (26~28%) in the distributions of the micro-beam sizes for all FDs. The average MLA micro-beam sizes increased from 220 μm to 397 μm with increasing FDs. In contrast, DOE exhibited relatively small deviations (2~5%) in the distributions of the micro-beam sizes for all FDs. The average DOE micro-beam sizes increased from 165 μm to 730 μm with increasing FDs, which is indicative of more FD-dependence. According to Fig. 4(c), the DOE group demonstrated that the overall micro-beam size increased more drastically with FD, and the two-fold larger overall size was observed at FD = 5 and 10 mm, compared to the MLA group ($p < 0.001$ vs. MLA).

Figure 5 shows H&E staining images of laser-treated skin with MLA and DOE at $H_0 = 3.0$ and 6.0 J/cm^2 at various FDs. According to Fig. 5(a), laser-induced vacuoles were generated with all the conditions. At FD = 0 mm, MLA created a group of large vacuoles randomly located in the epidermis and dermis at 3.0 and 6.0 J/cm^2. Deep vacuolization and consistent vacuole size were observed along with epidermal ablation at FD = 0 and 5 mm, but the vacuolization became shallower and smaller at FD = 10 mm. On the other hand, DOE generated a small number of mild intra-epidermal vacuoles along with superficial ablation on the epidermis at FD = 0 mm. A relatively high density of small vacuoles was uniformly distributed under the basal membrane at FD = 5 and 10 mm. Figure 5(b) compares depth, size, and number of laser-induced vacuoles in the skin at three FDs ($H_0 = 3.0$ J/cm^2). MLA presented a noticeable reduction in the vacuole depth at FD = 10 mm (321 ± 110 μm) whereas DOE generated the maximum vacuole depth at FD = 5 mm (349 μm at FD = 5 mm vs. 149 μm at FD = 0 mm and 236 μm at FD = 10 mm), which is still shallower than MLA ($p < 0.01$ at FD = 0 mm). In addition, MLA created up to two-fold larger vacuoles than DOE did (MLA = ~163 μm, DOE = ~64 μm; $p < 0.05$ at FD = 0 mm; $p < 0.001$ at FD = 5 and 10 mm vs. MLA). It was noted that the DOE-induced vacuole size was consistent and independent of FD. In spite of the minimum number of the vacuoles, DOE produced substantially more vacuoles with increasing FDs (FD = 5 and 10 mm). Table 1 summarizes a correlation of laser-induced parameters with H_0 and FD between MLA and DOE

Biomedical Optics EXPRESS

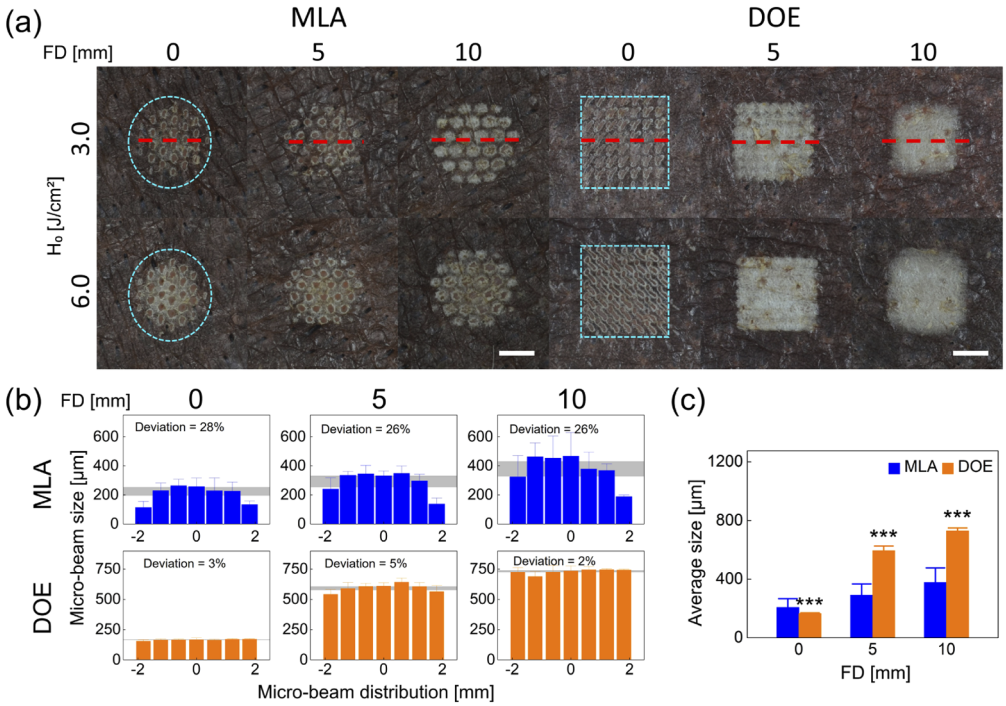

Fig. 4. Comparison of laser-induced responses in *ex vivo* pigmented porcine skin after irradiation with MLA and DOE at various radiant exposures (H_0 in J/cm^2) and focal depths (FD in mm): (a) top-view images of laser-irradiated skin surface, (b) spatial distributions of micro-beam sizes acquired from middle line (red dashed line) of macro-beam spots ($H_0 = 3.0$ J/cm^2), and (c) overall micro-beam sizes measured from macro-beam spot ($H_0 = 3.0$ J/cm^2). Note that cyan dashed lines in (a) indicate the boundary of the macro-beam spots on the skin surface (bar = 2 mm; ***$p < 0.001$ vs. MLA). Gray areas in (b) represent the deviations for the measured micro-beam sizes.

from the current tests. The correlation was determined by an increasing linear trend between each parameter and H_0 or FD (i.e., Y(+) when $R^2 \geq 0.85$).

Table 1. Correlation of laser-induced parameters with radiant exposure (H_0) and focal depth (FD)[a]

Parameters		H_0 (J/cm^2)		FD (mm)	
		MLA	DOE	MLA	DOE
Micro-beam spot on surface		Y (+)	Y (+)	Y (+)	Y (+)
Micro-bubble (in phantom)	Depth	Y (+)	Y (+)	Y (+)	N (max at 5 mm)
	Distribution	Gaussian-like	Flat-top	Gaussian-like	Flat-top
Vacuole (in tissue)	Depth	Y (+)	Y (+)	N (constant)	N (max at 5 mm)
	Size	N (constant)	N (constant)	N (constant)	N (constant)
	Density	Y (+)	Y (+)	N (constant)	N (max at 5 mm)
	Distribution	Non-uniform	Uniform	Non-uniform	Uniform

[a]Y = correlation; N = no correlation; + = increasing

Biomedical Optics EXPRESS

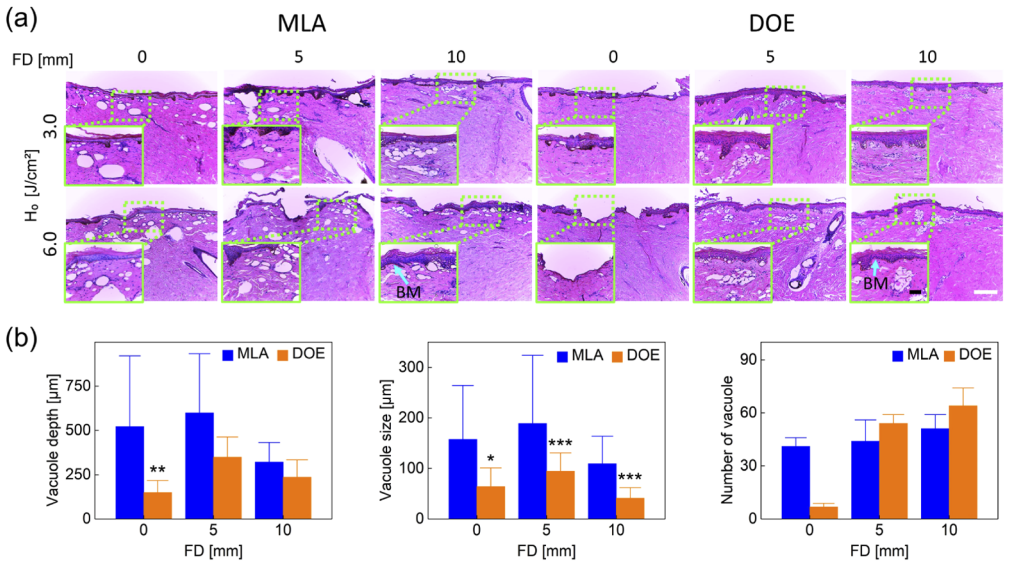

Fig. 5. Histological analysis of dark pigmented porcine skin tissue after irradiation with MLA and DOE at $H_0 = 3.0$ and 6.0 J/cm^2 at various FDs: (a) histological images of laser-irradiated skin tissue (100× and bar = 200 μm) and (b) quantitative comparison of laser-induced micro-bubble depth, size, and quantity measured from histology images ($H_0 = 3.0$ J/cm^2; *$p < 0.05$, **$p < 0.01$, ***$p < 0.001$ vs. MLA). Note that inlets (400× and bar = 50 μm) in (a) represent the magnified areas on the skin surface (light green dotted lines) and BM represents the position of basal membrane.

4. Discussions

The goal of the present study was to comparatively evaluate spatial LIOB effects of MLA and DOE on *ex vivo* pigmented porcine skin after irradiation of 1064-nm picosecond laser light at high energy settings. As the applied irradiance of each micro-beam ranged from 1.4×10^3 to 5.4×10^3 GW/cm^2, all the conditions consistently generated LIOB during the irradiation, regardless of target. High energy settings also enabled deep distributions of micro-bubbles in phantoms and laser-induced vacuoles in skin tissue (Figs. 3 and 5). However, it was noted that the extent of the micro-bubble distributions in the phantom was hardly reflected in that of the vacuolization in the tissue. Optical features of the target materials (relatively transparent phantom vs. turbid tissue) could account for the discrepancy in the spatial distributions. The preliminary measurements confirmed that DOE associated ~15% energy loss due to beam homogenization, compared to MLA. Thus, the applied pulse energy was regulated to compensate the existing energy loss with DOE and to deliver the equivalent output energy and H_0 (up to 6.0 J/cm^2) during the irradiation with MLA and DOE. However, due to a difference in the number of micro-beams (37 for MLA vs. 49 for DOE), MLA was estimated to have around 10% higher micro-beam energy than DOE under the same H_0. Both dimming paper and tissue-mimicking phantom validated that evenly-distributed micro-beams from DOE contributed to a flat-top distribution of micro-bubbles after the initiation of the DOE-assisted LIOB (Figs. 2 and 3). Thus, the multiple DOE micro-beams with high energy levels (i.e., up to 20.5 mJ/micro-beam) could result in deep and spatially-uniform formation of a higher density of constant vacuoles (~50 μm in size) under the basal membrane in the *ex vivo* porcine skin (300~400 μm in depth; Fig. 5). It should be noted that the deep and uniform vacuolization resulting from the DOE-assisted irradiation is expected to achieve consistent and predictable ablation of small target pigments underlying in

Biomedical Optics EXPRESS

the deep dermis [23,24]. Unlike the MLA group, the DOE group was markedly dependent on FD as the maximum depth and density of the laser-induced vacuolization occurred at FD = 5 mm (Fig. 5). The current findings implicate that DOE may need a deeper focusing to maximize the laser-induced vacuolization under various skin textures. Nevertheless, additional tests on different FDs will be necessary to elucidate the distance-dependent LIOB effects during the DOE-assisted picosecond laser treatment and eventually to optimize the treatment outcomes with consistent vacuolization in the deep dermis.

Increasing H_0 allowed the incident picosecond laser light to penetrate deeper in tissue but simultaneously accompanied irreversible lesion formation on the skin surface (Fig. 4). Particularly, MLA-assisted picosecond laser treatment at $H_0 = 6.0$ J/cm^2 vividly evidenced superficial ablation in epidermis and dermis (Figs. 4 and 5). In addition, higher FDs enlarged the micro-beams spots on the target surface (paper, phantom, and skin tissue), consequently losing the beneficial effect of fractional DOE beams. The current study applied multiple consecutive treatments (movement by 20 μm for ten times) with MLA and DOE on the skin in order to create a series of the vacuoles for quantitative comparison and visualization. However, the overlapping of the multiple micro-beams (~200 μm in diameter) contributed to accumulation of thermal injury on the tissue surface (Fig. 5(a)), resulting in a single expanded lesion formation (whitish discoloration; Fig. 4(a)). Moreover, unlike previous studies with single treatments at low energy settings, no evident plasma shielding [25,26] was observed during the current tests at high energy settings as the vacuolization depth increased with H_0 for both MLA and DOE (Table 1) [25]. The multiple treatments could have collectively suppressed the effect of the plasma shielding on the vacuolization (size and distribution) during the irradiation in light of accumulation of the LIOB-induced effect in the tissue. However, in order to confirm the current findings, additional single and multiple treatments with no beam overlapping should be ensued. Thus, the optimal treatment conditions will be identified in order to avoid or minimize unwanted ablation and/or thermal injury on the surface, to understand the plasma shielding effect at high energy settings, and to maintain the current spatial effects of LIOB with MLA and DOE. Interestingly, both the groups maintained the constant sizes of the vacuoles, irrespective of H_0 and FD (~160 μm for MLA vs. ~90 μm for DOE). In spite of around 40% smaller under the same conditions, DOE was associated with more confined distributions (FD = 5 mm), constant vacuole sizes with less deviation, and a higher number of the vacuoles, compared to MLA (Fig. 5(b)). Conceivably, the constant micro-beam patterns from DOE could maintain the equivalent amount of individual micro-beam energy and eventually to entail a large amount of consistent intra-dermal LIOBs in the tissue.

A number of previous studies reported effect of fractional picosecond laser treatment on *ex vivo* and human skin tissue [13,15,18,19,27]. Lee et.al. tested a 1064 nm picosecond laser with MLA (macro-beam diameter = 7 mm) at $H_0 = 2.8$ J/cm^2 on *ex vivo* porcine skin tissue. The study demonstrated that the MLA-assisted 1064 nm picosecond laser created the vacuoles (28 ± 10 μm in size) that were unevenly dispersed in the porcine skin (145 ± 26 μm in depth). In spite of the comparable vacuole size, the location was quite shallower than the current MLA results (size = ~163 μm and depth = ~350 μm at $H_0 = 3.0$ J/cm^2) possibly due to delivery of lower micro-beam energy associated with less numbers of micro-beam [13]. Yeh et.al. also examined a 1064 nm picosecond laser with MLA to generate the vacuoles (~50 μm in size located at 50~100 μm) in human skin at $H_0 = 1.2$ J/cm^2 [15]. The produced vacuoles were still smaller and shallowly distributed in the epidermis, compared to the current MLA results (up to 6.0 J/cm^2). The dimensional differences could result from various factors, including optical properties of skin type (human tissue vs. *ex vivo* porcine tissue), level of micro-beam energy (more than two-fold difference), and characteristics of LIOB (amount, depth, and size). On the other hand, Tanghetti et.al. presented that a 1064 nm picosecond laser with DOE induced the vacuoles of 40~60 μm in human epidermis at $H_0 = 1.1$ J/cm^2 [19]. Balu et.al. also visualized the laser–induced vacuoles

Biomedical Optics EXPRESS

of 49 ± 11 μm in the human epidermis by using multiphoton microscopy after irradiation of DOE-assisted 1064 nm picosecond laser light at $H_0 = 0.8$ J/cm^2 (macro-beam diameter = 6 mm) [27]. Despite the comparable vacuole size (40~60 μm), the previous DOE studies confined the laser-induced vacuolization merely to the epidermis as low micro-beam energy or H_0 was applied. On the other hand, the present study tested high pulse energy settings ($H_0 = 1.5$~6.0 J/cm^2) explore the dependence of the intra-dermal LIOB effects in the skin on MLA and DOE and eventually to assess a potential capability of ablating deeply-located melanin pigments. In spite of a strong dependence on FD, the DOE group revealed the uniform distributions of a high density of the laser-induced vacuoles with consistent size (~78 μm) under the basal membrane (300~400 μm in depth) in skin. A ramification of the current findings may suggest a treatment capacity of the DOE-assisted picosecond laser treatment for deep skin pigments at high energy settings. Further tests with human skin should be followed to confirm the current findings and to warrant clinical benefits for dermatologists.

Although DOE-assisted picosecond laser demonstrated more uniform distributions of laser-induced vacuoles under the basal membrane, experimental limitations still remain for clinical translation. All the targets used in the experiments had a relatively flat surface for better optical coupling with minimal specular reflection. However, MLA can deposit and employ the incident laser energy on a rough surface whereas DOE can work well on a flat surface. Thus, as a significant clinical parameter, various surface conditions (e.g., smooth vs. rough) should be examined to validate the current findings with MLA and DOE. As the present study tested porcine pigmented skin, *ex vivo* tissue hardly reflects *in vivo* and human tissue conditions in terms of melanin distributions, water contents, blood perfusion, and skin temperature. In fact, variations in optical properties contingent on skin color may vary thresholds and characteristics of LIOB on the skin tissue. Lack of dermal blood flow can hardly evaluate superficial dermal hemorrhage particularly after laser treatment at high energy settings. The current study merely used the dark pigmented porcine skin to ensure the initiation of LIOB for all the conditions. Thus, additional skin types/colors should be assessed to elucidate the dependence of the DOE-induced LIOB on the melanin contents and distributions. Only three different FDs were selected to simulate the effect of human skin texture (i.e., surface condition) on the intra-dermal LIOB responses. However, the nonlinear dependence of the laser-induced vacuolization on FD (Fig. 5) needs to examine various treatment distances for warranting the optimal clinical outcomes of the DOE-assisted laser treatment. Therefore, for potential clinical translation, further studies will be performed to validate the current findings in *in vivo* porcine models with multiple skin colors in terms of degree of pigment removal, acute and chronic responses of laser-treated skin with MLA and DOE, and recurrence rate of the treated pigments.

5. Conclusions

The current study compared spatial effects of LIOB with MLA and DOE on *ex vivo* skin tissue by using a picosecond laser system at high energy settings. In spite of strong dependence on FD, DOE generated spatially-uniform distributions of micro-beams and resulted in homogenous laser-induced vacuolization under the basal membrane after generation of intra-dermal LIOB. Further investigations will validate the potential efficacy and safety of the DOE-assisted picosecond laser treatment in *in vivo* porcine skin models for clinical translation.

Funding

Ministry of SMEs and Startups (S2780486).

Biomedical Optics EXPRESS

Acknowledgments

This work was supported by the Technology Development Program (S2780486) funded by the Ministry of SMEs and Startups (MSS, Korea).

Disclosures

The authors have no conflict of interest related to this article.

References

1. P. E. Grimes, "Melasma. Etiologic and therapeutic considerations," Arch. Dermatol. **131**(12), 1453–1457 (1995).
2. A. C. Handel, L. D. Miot, and H. A. Miot, "Melasma: a clinical and epidemiological review," An. Bras. Dermatol. **89**(5), 771–782 (2014).
3. O. A. Ogbechie-Godec and N. Elbuluk, "Melasma: an Up-to-Date Comprehensive Review," Dermatol. Ther. **7**(3), 305–318 (2017).
4. G. H. Fisher and R. G. Geronemus, "Short-term side effects of fractional photothermolysis," Dermatol. Surg. **31**, 1245–1249 (2006).
5. E. M. Graber, E. L. Tanzi, and T. S. Alster, "Side effects and complications of fractional laser photothermolysis: experience with 961 treatments," Dermatol. Surg. **34**, 301–307 (2008).
6. D. J. Goldberg, "Laser treatment of pigmented lesions," Dermatol. Clin. **15**(3), 397–407 (1997).
7. S. Watanabe, R. R. Anderson, S. Brorson, G. Dalickas, J. G. Fujimoto, and T. J. Flotte, "Comparative studies of femtosecond to microsecond laser pulses on selective pigmented cell injury in skin," Photochem. Photobiol. **53**(6), 757–762 (1991).
8. U. Paasch and S. Grunewald, "2018 update on dermatologic laser therapy: Part 1 - epilation, vascular lesions and pigments," JDDG: Journal der Deutschen Dermatologischen Gesellschaft **16**, 1417–1423 (2018).
9. P. K. Kennedy, D. X. Hammer, and B. A. Rockwell, "Laser-induced breakdown in aqueous media," Prog. Quantum Electron. **21**(3), 155–248 (1997).
10. B. Varghese, V. Bonito, M. Jurna, J. Palero, and M. H. Verhagen, "Influence of absorption induced thermal initiation pathway on irradiance threshold for laser induced breakdown," Biomed. Opt. Express **6**(4), 1234–1240 (2015).
11. A. G. Doukas, A. D. Zweig, J. K. Frisoli, R. Birngruber, and T. F. Deutsch, "Non-invasive determination of shock wave pressure generated by optical breakdown," Appl. Phys. B **53**(4), 237–245 (1991).
12. C. Y. Hwang and C. C. Chen, "Serial change in laser-induced optical breakdown by 1064-nm Nd: YAG picosecond laser," Photodermatol., Photoimmunol. Photomed. **36**(1), 63–64 (2020).
13. H. C. Lee, J. Childs, H. J. Chung, J. Park, J. Hong, and S. B. Cho, "Pattern analysis of 532- and 1,064-nm picosecond-domain laser-induced immediate tissue reactions in ex vivo pigmented micropig skin," Sci. Rep. **9**(1), 4186 (2019).
14. L. Kirsanova, E. Araviiskaia, M. Rybakova, E. Sokolovsky, A. Bogatenkov, and F. Al-Niaimi, "Histological characterization of age-related skin changes following the use of picosecond laser: Low vs high energy," Dermatol. Ther. **33**(4), e13635 (2020).
15. Y. T. Yeh, J. H. Peng, and P. Peng, "Histology of ex vivo skin after treatment with fractionated picosecond Nd:YAG laser in high and low-energy settings," J. Cosmet. Laser. Ther. **22**(1), 43–47 (2020).
16. C. Kopp, L. Ravel, and P. Meyrueis, "Efficient beamshaper homogenizer design combining diffractive optical elements, microlens array and random phase plate," J. Opt. A: Pure Appl. Opt. **1**(3), 398–403 (1999).
17. D. J. Kang, J. P. Jeong, and B. S. Bae, "Direct photofabrication of focal-length-controlled microlens array using photoinduced migration mechanisms of photosensitive sol-gel hybrid materials," Opt. Express **14**(18), 8347–8353 (2006).
18. E. A. Tanghetti, "The histology of skin treated with a picosecond alexandrite laser and a fractional lens array," Lasers Surg. Med. **48**(7), 646–652 (2016).
19. E. Tanghetti Md and J. Jennings, "A comparative study with a 755 nm picosecond Alexandrite laser with a diffractive lens array and a 532 nm/1064 nm Nd:YAG with a holographic optic," Lasers Surg. Med. **50**(1), 37–44 (2018).
20. L. N. Geraghty and B. Biesman, "Clinical evaluation of a single-wavelength fractional laser and a novel multi-wavelength fractional laser in the treatment of photodamaged skin," Lasers Surg. Med. **41**(6), 408–416 (2009).
21. Y. Shimojo, T. Nishimura, H. Hazama, T. Ozawa, and K. Awazu, "Measurement of absorption and reduced scattering coefficients in Asian human epidermis, dermis, and subcutaneous fat tissues in the 400- to 1100-nm wavelength range for optical penetration depth and energy deposition analysis," J. Biomed. Opt. **25**(04), 1–14 (2020).
22. X. Ma, J. Q. Lu, H. Ding, and X. H. Hu, "Bulk optical parameters of porcine skin dermis at eight wavelengths from 325 to 1557 nm," Opt. Lett. **30**(4), 412–414 (2005).
23. L. Habbema, R. Verhagen, R. Van Hal, Y. Liu, and B. Varghese, "Minimally invasive non-thermal laser technology using laser-induced optical breakdown for skin rejuvenation," J. Biophotonics **5**(2), 194–199 (2012).
24. J. A. Brauer, V. Kazlouskaya, H. Alabdulrazzaq, Y. S. Bae, L. J. Bernstein, R. Anolik, P. A. Heller, and R. G. Geronemus, "Use of a picosecond pulse duration laser with specialized optic for treatment of facial acne scarring," JAMA Dermatol. **151**(3), 278–284 (2015).

Biomedical Optics EXPRESS

25. A. Vogel, K. Nahen, D. Theisen, and J. Noack, "Plasma formation in water by picosecond and nanosecond Nd: YAG laser pulses. I. Optical breakdown at threshold and superthreshold irradiance," IEEE J. Sel. Top. Quantum Electron. **2**(4), 847–860 (1996).
26. J. A. Aguilera, C. Aragón, and F. Peñalba, "Plasma shielding effect in laser ablation of metallic samples and its influence on LIBS analysis," Appl. Surf. Sci. **127-129**, 309–314 (1998).
27. M. Balu, G. Lentsch, D. Z. Korta, K. Konig, K. M. Kelly, B. J. Tromberg, and C. B. Zachary, "In vivo multiphoton-microscopy of picosecond-laser-induced optical breakdown in human skin," Lasers Surg. Med. **49**(6), 555–562 (2017).